KINGDOM OF SAUDI ARABIA
Northern Border University (NBU)
Journal of the North for Basic & Applied Sciences(JNBAS)
p - ISSN : 1658 -7022 / **e-ISSN:** 1658 - 7014
www.nbu.edu.sa
s.journal@nbu.edu.sa

High Aspect Ratio CeO_2 Nanocrystals Decorated Polyaniline Heterostructure for Dual Function: Green Remediation of Water Pollutants and Microbial Pathogens

M. Shamshi Hassan
Department of Chemistry, Faculty of Science, Al-Baha University, Al-Baha 65799, Saudi Arabia.

(**Received:** : 13th June 2026; **Accepted:** 13th September 2026)

Abstract
The textile production companies are main tracks to water contamination owing to massive utilization of synthetic colorants, which are often resistant to degradation and pose significant environmental and health risks. Rhodamine 6G (R6G) dyes which are one of the significant water pollutants, have a complex structure and are lethal if ingested or inhaled in substantial amounts. Similarly, food-borne infections are also key concerns of community well-being, internationally. This study introduces a novel method to boost antimicrobial effectiveness of CeO_2 decorated PANI composite against food pathogens and simultaneously aid in removing hazardous effluents such as R6G from wastewaters. The CeO_2 decorated PANI heterostructure, therefore, grips enormous potential in preserving two essential pillars of sustenance viz., water and food. CeO_2 decorated PANI heterostructure have been amalgamated via in situ deposition oxidative polymerization method. Samples were characterized in detail using sophisticated procedures, such as XRD, SEM-EDX, FT-IR and UV-Vis. The CeO_2-PANI heterostructure exhibit enhanced photocatalytic performance under visible light. The composite also showed strong antimicrobial activity against representative bacteria and fungus, mainly through ROS generation and cell membrane disruption. These nanocomposites offer a cost-effective, scalable approach for advanced photocatalytic destruction of bacteria and fungi which is desirable in diverse healthcare applications.

Keywords: Nanocomposite; Water pollutants; Antimicrobial; Pathogens; Photocatalyst

1658-7022© JNBAS. (1448 H/2026). Published by Northern Border University (NBU). All Rights Reserved.

(*) **Corresponding Author**:
M. Shamshi Hassan
Department of Chemistry, Faculty of Science, Al-Baha University, Al-Baha 65799, Saudi Arabia.

E-mail: imshamshi@gmail.com (M. S. Hassan)
Phone no: +966536913920

DOI: 10.12816/0062684

1. Introduction

Globally water pollution is a perilous problem, imposing incessant appraisal and upgrading water resources. It is one of the major contributors to sickness and mortality. Both developed and developing countries experience momentous trials in sustaining water quality. Water worth is spoiled by various of natural and human activities (Chaudhry & Malik, 2017). In this direction the textile industry significantly contributes to water pollution via artificial colorants, resulting environmental instabilities, hazardous impact on marine flora and fauna, and abridged water eminence from dye-loaded wastewater emancipation. Nonetheless, the textile industry contributes considerably to environmental pollution, principally owing to excessive use of synthetic dyes which impart vivacious colors to textiles, often very complicated to disintegrate, therefore, retain in atmosphere, resulting hazardous consequences (Kumbhar, Shingare, Bagal, Suryawanshi, & Mane, 2025). Heterogeneous photocatalysis is a progressive oxidation procedure and is topic of rigorous investigations subjected to air and water cleansing. However, application of light energy for translation into chemical vigor and safeguarding environmental sterility is a challenge. A lot of investigations are being carried out to expand photocatalytic process established on semiconductor (Algethami et al., 2023; Hassan et al., 2022). So, nowadays, considerable attention has been given to conducting polymers as they fulfil anticipated standards which brand them perfect for an active catalyst matrix (Q. Wang et al., 2013). Nanoceria, one of the significant rare earth oxides has broadly been exploited in catalytic and biological fields owed to its inimitable redox (Ce^{3+} and Ce^{4+}) and robust buffering characteristics (Phanichphant, Nakaruk, & Channei, 2016; Samai & Bhattacharya, 2018). Moreover, nowadays considerable attention has been given to conducting polymers as they fulfil anticipated standards which brand them perfect for an active catalyst matrix (Q. Wang et al., 2013). The mortality frequency is intensifying worldwide owing to swift development of bacterial and fungal infections, as well as prevalent occurrence of resistant microorganisms. It has been foretold that approximately 10 million people will expire yearly from these infections, by 2050, and treatment expenses may reach USD 100 trillion. Nonetheless, during the year 2014, World Health Organization (WHO) acknowledged advancement of antimicrobial resistant microorganisms as a grave peril to universal well-being (Ghodake, Koyale, Patil, Patil, & Delekar, 2025). Salmonellosis is one of the most predominant foodborne sicknesses causing roughly 93.8 million food related infections and 155,000 losses globally on yearly basis. The transmission of non-typhoid Salmonella contagion to beings can happen via incorporation of foodstuff or water soiled with excreta of infested fauna, interaction with diseased fauna or by ingesting food of diseased creatures (Eng et al., 2015). The genera Salmonella is an adherent of Enterobacteriaceae family, and it comprises Gram-negative, whipped, non-sporulating, and facultative bacteria that normally grow from 35-37 °C. S. Typhimurium is pre-dominant serovar in environment, allied with foodborne epidemics equally in developing and developed nations (Mohammed, 2017). Similarly, Staphylococcal food related disease (SFD) is also most prevalent food-borne ailments resultant of infection of foodstuffs by S. aureus enterotoxins. Additionally, it is most common source of testified food-borne illnesses in USA. Even though numerous Staphylococcal enterotoxins (SEs) have been recognized, however, SEA, an extremely heat resistant, is prevalent basis of SFD internationally. Epidemic surveys have initiated that inappropriate food management in retail industry justify most of SFD outbursts (Kadariya, Smith, & Thapaliya, 2014). Staphylococcus aureus is a commensal and an opportunistic pathogen as well proficient to spread wide-ranging infestations, for instance; insignificant dermal infections to acute life-threatening hostile illnesses (Kadariya et al., 2014; Lowy, 1998). Currently, nanotextured fibers and tubes inherited with antimicrobial potential are of tremendous demand owing to their extensive antibiotic resistance for diverse pathogens. These nanotextured materials are usually based on metal or metal oxide nanoparticles that have been in practice since centuries (Maliszewska & Czapka, 2022). Furthermore, in this direction, the cerium oxide (CeO_2) and polyaniline (PANI) are two important materials that have attained noteworthy consideration due to their exceptional assets and impeding usage in diverse arena. CeO_2 is a rare earth metal oxide that displays outstanding catalytic, optical, and electronic properties, while PANI is a conductive polymer that possesses good mechanical strength, thermal stability, and electrical conductivity. The amalgamation of these two materials in a heterostructure has shown promising results in photocatalysis and antimicrobial applications in present study. Therefore, this newly designed heterostructure not only constrains foodborne pathogens but can also prevent biofilm formation on surfaces, also a key factor in reducing chemical and biological long-term contamination in water systems.

2. Experimental

2.1 Chemicals

Aniline monomer, ammonium per-sulfate (APS) and Oleylamine (70%) were procured from Sigma-Aldrich and citric acid were brought from Showa Chemicals Ltd., Japan. Cerium (III) nitrate hexahydrate (99%) and Diphenyl ether (99%) were purchased from Samchun chemicals, South Korea.

2.2 Synthesis of samples

2.2.1 Synthesis of CeO_2 Nanocrystals

CeO_2 Nanocrystals were synthesized using previously

established methodology (Hassan et al., 2016) with desired alterations. Cerium nitrate hexahydrate (1.7 g) was combined with oleylamine (20 ml) at room temperature in a three-neck flask with stirring at 400 rotation per minute (RPM). After raising the temperature to 90 °C, a clear solution was occasionally obtained (pH~9). At 90 °C, diphenyl ether (3.0 ml) was added to the same solution. After two hours, the solution temperature increased 320 °C and it was allowed to age for two hours. A colloidal black fluid is produced. To precipitate the solution, 100 mL of ethanol was added after the solution had cooled down. Finally, the solution was centrifuged, the finished product was dispersed into toluene or hexane.

2.2.2 Synthesis of PANI NTs

Typically, 500 ml of distilled water was combined with 0.1 M of aniline, and then 4.0 g of citric acid was supplemented to make solution. Then, in a 1:1 weight percentage ratio, the CeO_2 NCs were added to the mixture. Simultaneously, a 0.1M APS aqueous solution was stirred into the previous solution (Jeong et al., 2014). After that, the sample was refrigerated 24 hours at 4 °C. High-suspended stability PANI-CeO_2 composite suspension was created. After filtration the composite suspension washed three times with distilled water and one time with ethanol to get rid of any remnants, the finished product was vacuum-dried overnight at 60 °C.

2.2.3 Synthesis of CeO_2 NCs-PANI NTs composite

For the synthesis of composite sample, CeO_2 NCs were added (1:1 w/w) to the mixture of aniline and citric acid, then APS was added for polymerization. Rest of the process was identical as described above for pure PANI nanotubes synthesis.

2.3 Characterization and Photocatalysis

The XRD of produced heterostructure was documented on a Rigaku/Max-3A X-ray diffractometer with CuK radiation (λ=1.5418 Å), operational voltage and current has been insisted at 30 kV and 40 mA, correspondingly (Amna et al., 2012). To inspect the structural features and chemical composition, the composite was homogeneously squirted on aluminum foil and imaging was carried out at diverse intensifications by field (FESEM-EDX, JEOL JSM6700, Japan) and transmission electron microscopy (TEM, H-7650, Hitachi, Japan). The Fourier transform infrared (FTIR) spectra using KBr pellet technique (Varian FTS 1000) was acquired. The light absorbance of heterostructures was determined by UV-Vis diffused reflectance spectrum (UV-DRS, 525 Shimadzu).

To perform photocatalytic degradation, 2.5 mg of materials were continuously stirred into 250 mL of R6G solution (10 ppm). Before irradiating slurry with visible light ($\lambda > 400$ nm), it was aerated for 30 min to accomplish adsorption equilibrium. Photocatalytic studies were conducted at room temperature. At predetermined intervals, representative samples were captured from suspension and centrifuged right away at 12,000 rpm. With the help of UV-Vis spectrophotometer (Shimadzu UV-3101) absorbance of the R6G solution was assessed.

2.4 Growth inhibition studies of CeO_2-PANI NTs

The antibacterial efficacy of CeO_2-PANI NTs was evaluated through growth inhibition assays, based on previously described methodologies (Amna, 2023; Amna et al., 2013) with applicable amendments against two representative foodborne bacteria, S. aureus KCCM 11256 and S. typhimurium KCCM 11862, procured from KCCM, South Korea. To begin with, axenic bacterial cultures were made to proliferate by colonies from Tryptic Soy Agar (TSA) into Tryptic Soy Broth (TSB; pH 7.3) and incubated at 37 °C for 18 h. Bacteriological advancement was monitored at specific intervals using a UV visible spectrophotometer (UV-2550, Shimadzu, Japan) via optical density (OD). For antibacterial assay, 1 mL of homogenous revived bacterial inocula was added to fresh broth augmented with variable concentrations of CeO_2-PANI NTs (0, 100, 200, and 400 µg/mL). All experimental flasks were upheld as aforementioned under constant agitation at 150 rpm. The influence of CeO_2-PANI NTs on bacterial propagation/inhibition was administered spectrophotometrically as a function of time, aiding quantitative assessment of growth inhibition(Shamshi Hassan et al., 2024).

2.5 Antimycotic activity of CeO_2-PANI NTs

A clinical isolate of Candida albicans (ATCC 10231) used in this study was maintained and cultured according to previously established protocols (Jalal, Ansari, Ali, Khan, & Rehman, 2018). The antifungal activity of CeO_2-PANI NTs was evaluated using a range of concentrations. Minimum fungicidal concentrations (MFCs) were determined on Sabouraud Dextrose Agar (SDA) plates, following method described by (Alghamdi et al., 2024; Jalal et al., 2016) with appropriate adjustments. Fungal growth was monitored after a 72h incubation period, using a two-fold serial dilution of CeO_2-PANI ranging from 0 to 800 µg/mL.

3. Results and discussion

The X-ray diffractograms of PANI, CeO_2 and PANI@CeO_2 composite are referred in Fig. 1. The broad characteristic apices at 20-25 degree indicate amorphous polyaniline phase (Fig. 1a) (Jeong et al., 2014). The diffraction peaks at 28.31, 32.91, 47.31, 56.01, 59.61 and 69.01 correspond to cubic configuration of CeO_2 (Hassan et al., 2016).

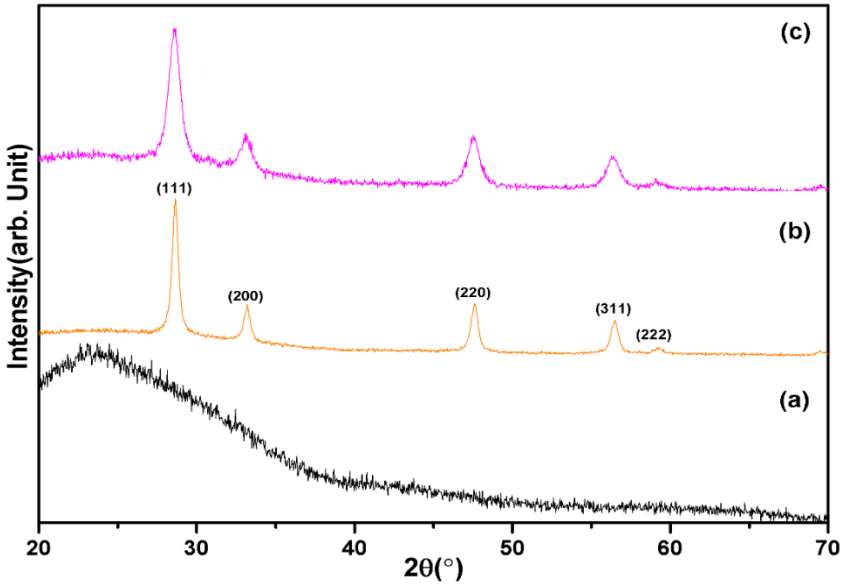


Figure 1. XRD pattern of (a) PANI (b) CeO_2 and (c) CeO_2-PANI heterostructure

High intensity of peaks proved crystallinity of CeO_2 (Fig. 1b). On the other hand, PANI@CeO_2 composite is composed of all the characteristic peaks of phase CeO_2 whereas distinguishing peaks of PANI were not detected in composite due to amorphous nature of PANI (Fig. 1c). The crystallite sizes of pristine CeO_2 and the CeO_2-PANI heterostructure were estimated using the Debye-Scherrer equation based on the prominent CeO_2 (111) diffraction peak. The calculated crystallite sizes were approximately 7.98 nm for CeO_2 and 13.65 nm for the CeO_2-PANI heterostructure, indicating that the incorporation of PANI did not significantly alter the crystallite size of CeO_2. During heterostructure formation, PANI may modify the local chemical environment around CeO_2 particles, allowing smaller CeO_2 crystallites to grow or reorganize into larger crystalline domains. The surface morphology of the composite powders can be observed by FESEM analysis. Figure 2a determines SEM views of pure PANI having tubular structures. As shown in Figure 2b, pure CeO_2 is rounded in shape and exhibited nano-size. Whereas Fig 2(c, d) shows the images of CeO_2-PANI, it clearly demonstrated the heterostructure having CeO_2 nanocrystals distributed over the PANI nanotube.

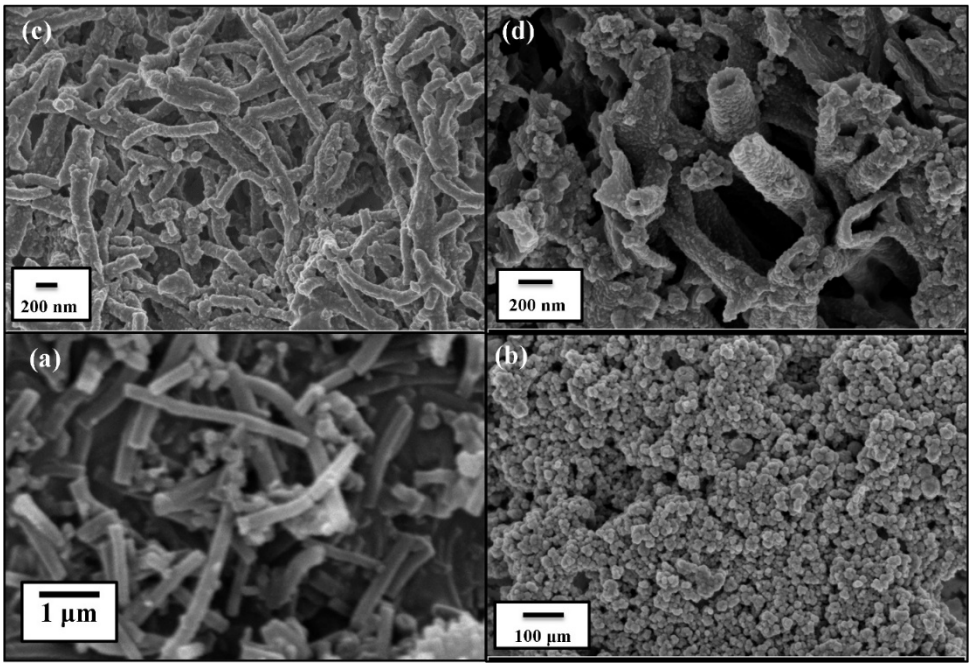


Figure 2. FESEM images of (a) pure PANI (inset shows high magnification), (b) CeO_2 and (c, d) CeO_2-PANI NTs at different magnifications

These results were further explained and confirmed by TEM images (Fig. 3). Fig. 3a shows TEM micrograph of CeO_2 sample which clearly shows the formation of spherical nanocrystals having diameters around 7-8 nm. Whereas PANI shows the tubular structure having diameter of the nanotube, ranges between 100 to 200 nm (Inset Fig. 3a). Fig. 3 (b, c) shows the high-resolution TEM appearance of CeO_2-PANI heterostructure. Microstructures reflected two distinct pictures, one having dark crystalline structure of CeO_2 and another image shows amorphous PANI. The SAED pattern of composite displays the multi-crystalline nature of composite (Fig. 3d).

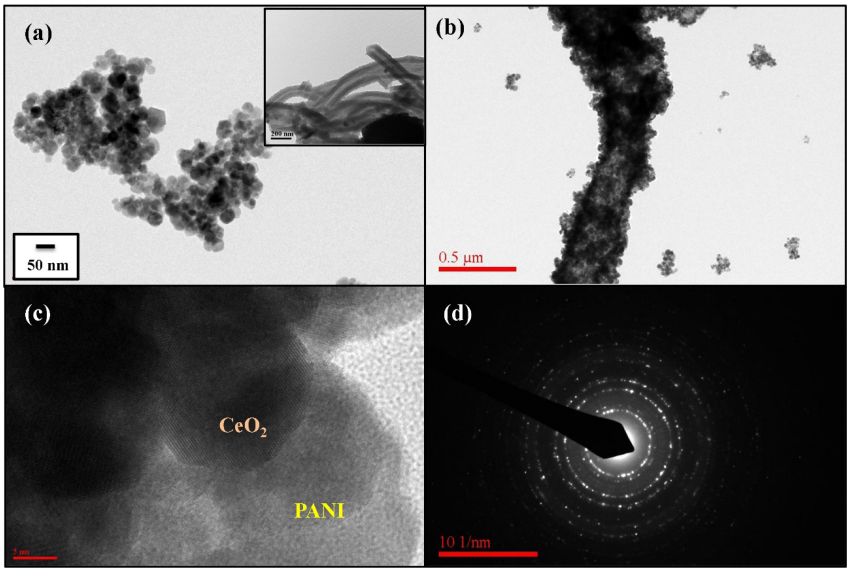
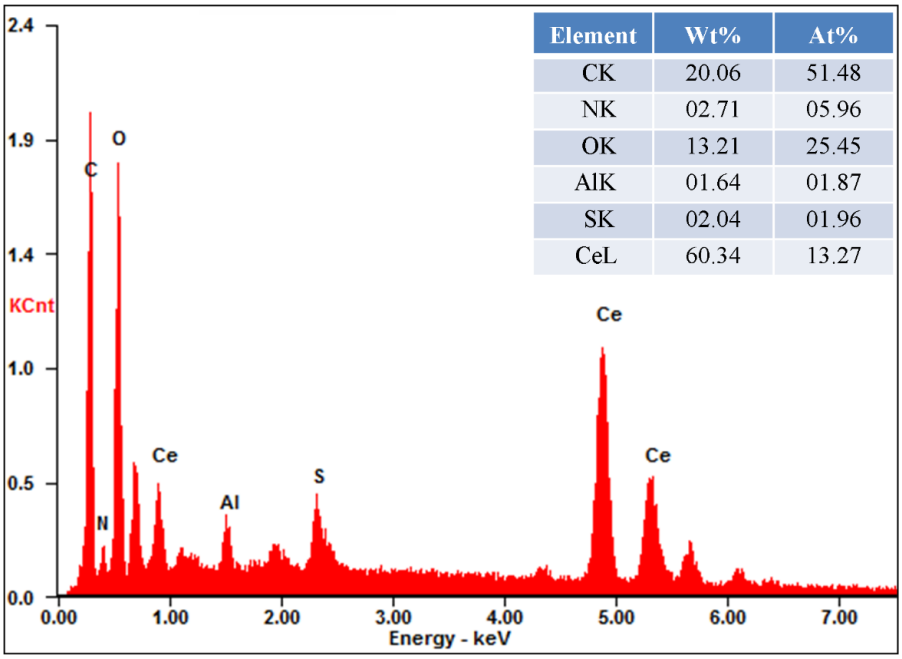


Figure 3. TEM image of (a) CeO_2 NCs (Inset shows image of PANI NTs) (b) CeO_2-PANI heterostructure (c) HR-TEM image and (d) SAED pattern of CeO_2-PANI

EDS analysis was employed to determine the composition of heterostructure (Fig. 4). The sample contains Ce, C, N and O elements, which further authorizes the presence of CeO_2 particles on exterior of PANI nanotubes. Appearance of Sulphur is ascribed to remnants of ammonium peroxodisulphate, utilized as an oxidant in preparation of PANI. Aluminum peak is due to the sampling of EDX was done on aluminum foil.



Element	Wt%	At%
CK	20.06	51.48
NK	02.71	05.96
OK	13.21	25.45
AlK	01.64	01.87
SK	02.04	01.96
CeL	60.34	13.27

Figure 4. EDX spectrum of CeO_2-PANI heterostructure

FT-IR spectral lines for pure PANI, CeO_2 and CeO_2-PANI heterostructure are revealed in Figure 5. Figure 5a describes representative FTIR of PANI. Characteristic peaks at 1567 cm^{-1} and 1493 cm^{-1} were assigned to C=N widening of quinoid and C=C stretching of the benzoid rings. The stretches at 1240 and 1298 cm^{-1} link to C-N expanding in benzene and quinone rings. The stretch out peak of quinone ring is confirmed by absorption crest (1148 cm^{-1}). Crowning at 820 cm^{-1} is C-H bond-bending vibration of disubstituted benzene ring outward surface (He, Li, & Guo, 2012; Singu, Srinivasan, & Pabba, 2011). Presence of widening band sprinted around 400 cm^{-1} proves development of Ce-O bond (Ho, Yu, Kwong, Mak, & Lai, 2005) (Fig. 5b). Fig. 5c shows the spectrum of composite samples having all the peaks of CeO_2 and PANI with little shift in the peak position to the higher wave number side. All the spectrum demonstrated a wide peak at 3450 cm^{-1}, linking to-OH stretching of water and hydroxyl clusters.

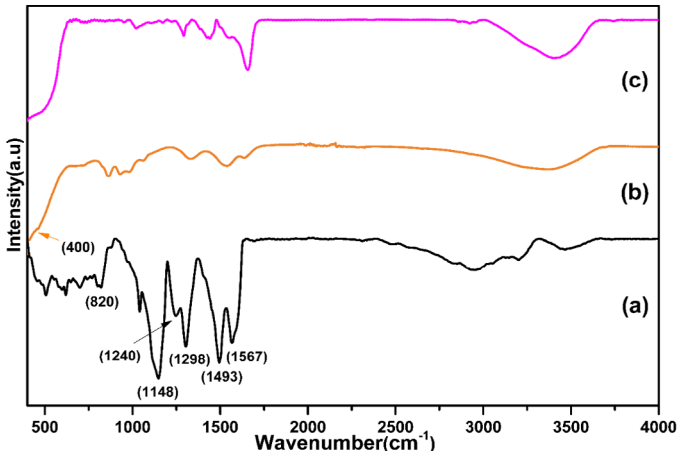


Figure 5. FT-IR spectra of (a) PANI (b) CeO_2 and (c) CeO_2-PANI heterostructure

UV-vis diffuse reflectance spectra of PANI, CeO_2 and CeO_2-PANI heterostructure are illustrated in Fig. 6. PANI (Fig. 6a) indicates two typical crests centered at about 350 and 680 nm wavelengths. The absorption at 380 nm is owed to p-p* transition on polymer and second band at 680 nm attributed to exciton transition (Guo et al., 2013). The spectrum of CeO_2 shows that it has high absorption in UV section and weak absorption in visible light (Fig. 6b). The calculated band gap energy is 3.15 eV (H. Wang, Yang, Yu, & Peng, 2011). Compared to CeO_2, CeO_2-PANI showed absorption to higher wavelength with high intensity (Fig. 6c). The value of band gap energy calculated from spectrum was 3.05 eV. So, the heterostructure showed narrow band gaps and broadened light absorption. The change in absorption of CeO_2-PANI composite is attributed to development of hydrogen bonding between CeO_2 crystals and NAH groups in PANI (Li et al., 2003). These CeO_2-PANI heterostructures have been applied to remove R6G under visible light. Dyes are lethal in nature, but their stoppage is not possible owing to their diverse applications. These dyes possess complicated configurations having multiple functional groups. Furthermore, besides having hazardous impact on marine existence, these dyes are carcinogenic also. Therefore, their eradication from waterbodies is essential. The colored dyes accumulation impedes sunlight penetrating water, thus disturbing the life of water ecosystems significantly. Even these wastewater reservoirs are not suitable for land irrigation. In this regards the photocatalytic dilapidation is believed to be a green approach that transforms photonic energy into useful chemical energy (Haleem et al., 2024).

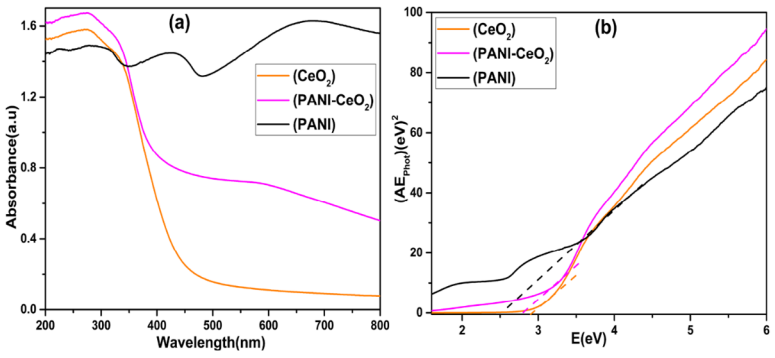


Figure 6. (a) UV-Vis diffuse reflectance spectra and (b) plot of Kubelka-Munk function vs. photon energy of the pure PANI, CeO_2 and CeO_2-PANI heterostructure

The photodegradation of PANI, CeO_2 and CeO_2-PANI materials were assessed via disintegration of R6G in visible light. When irradiated by visible light, PANI and CeO_2 exhibit photocatalytic activity of about 15% and 45% of R6G decomposition in 150 min. Compared with PANI and CeO_2, the CeO_2-PANI composite materials possess better photocatalytic properties (Fig.7a). Approx. 76% R6G can be photodegraded by the composite photocatalyst under the same condition. The high efficiency can be inferred to the parting of photogenerated electron-hole pairs owing to development of a p-n heterojunction between CeO_2 and PANI (Yu et al., 2018). Nonetheless, it has been well identified that semiconductors have a small band gap between conduction and valence bands, thus the electrons could easily be excited from the VB to CB after illumination (Haleem et al., 2024). Furthermore, to investigate the reaction kinetics of R6G degradation, the pseudo-first-order kinetic reaction eqn. (1) was applied in the experiments:

$$\ln(C_0/C) = k_{app}t \quad (1)$$

Where C_0 is original concentration of R6G, C is concentration of R6G at different reaction time and k_{app} is pseudo-first-order rate constant (min^{-1}). The corresponding linear transforms in $\ln(C_0/C)$ as a function of illumination time are given in Fig. 7b. The value of calculated k_{app} for PANI, CeO_2 and CeO_2-PANI composite were 0.0007 min^{-1}, 0.004 min^{-1} and 0.01 min^{-1}, respectively. The degradation rate constant of CeO_2-PANI was around 14.2 and 2.5 times higher than those of PANI and CeO_2, respectively.

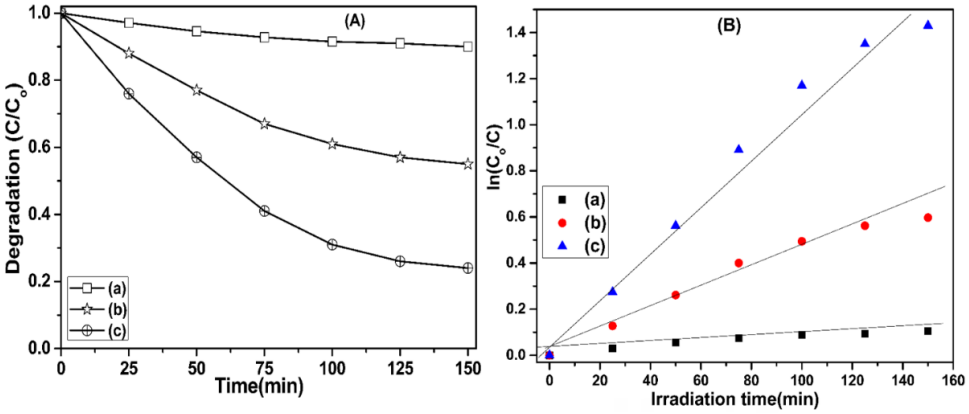


Figure 7. (A) Photocatalytic degradation and (B) Fitted pseudo first-order kinetics for degradation of R6G dye by (a) PANI (b) CeO_2 (c) CeO_2-PANI heterostructure

To investigate the recyclability of optimized photocatalysts, CeO_2-PANI were used for five photocatalytic cycles of degradation of R6G in aqueous solution. After each photocatalytic degradation, the photocatalyst was separated, washed and dried, and used for further run without any treatment. Fig.8 shows the recycling test of CeO_2-PANI heterostructure for degradation of R6G. The R6G degradation shows a bit decrease in efficiency with increase in cycle number but still efficiency was good even after 5 cycles. The R6G degradation rates were 76%, 75%, 74%, 73% and 73%, respectively showing better stability of photocatalyst.

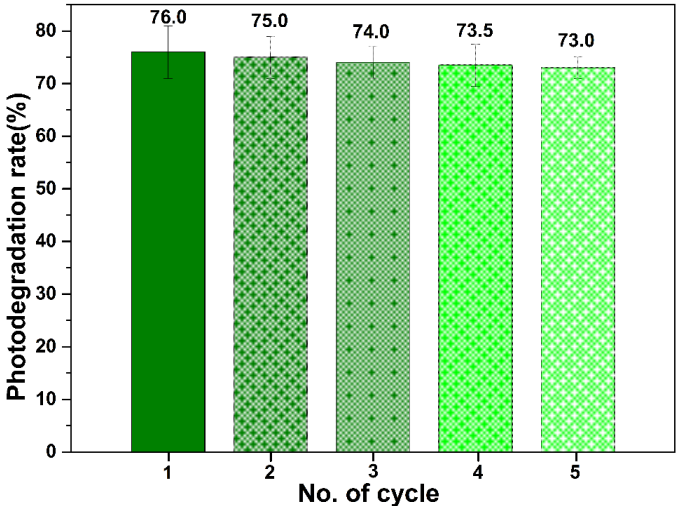


Figure 8. Photocatalytic efficiency of R6G dye by CeO_2-PANI heterostructure in cycles

Scheme 1 depicts a proposed hypothesis of charge separation and enhancement of photodegradation of CeO_2-PANI heterostructure (Fig.9). The CB of CeO_2 was lower than LUMO of PANI, so it works as a reservoir for photogenerated electrons in CeO_2-PANI photocatalyst. The VB CeO_2 was lower than HOMO of PANI, so the later could act acceptor for photogenerated holes (Cho, Park, Hwang, & Choi, 2004; Lotfi, Ouardi, Ahsaine, & Assani, 2022; Sharma & Khare, 2018; Turkten, Karatas, Kurumoglu, & Gurkan, 2025). Therefore, the CeO_2 and PANI can be excited by visible light and the electrons from PANI may be transferred to CeO_2 CB. Simultaneously, holes in VB of CeO_2 can spontaneously injected to HOMO of PANI. Consequently, the photogenerated electrons and holes rolled in opposite ways, reducing the chances of recombination, Therefore, reaction triggers development of super oxide radical ion and hydroxyl radical, ultimately ensuing high photodegradation efficiency which leads to degradation of dye (Turkten et al., 2025).

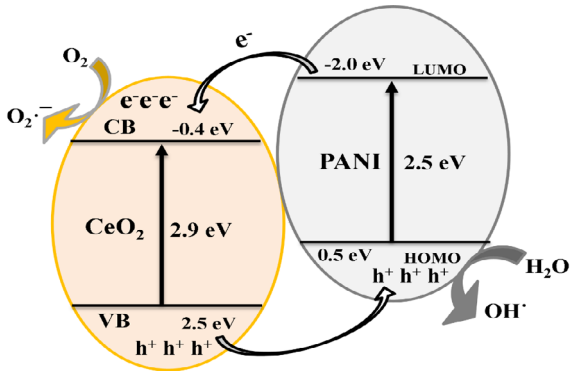


Figure 9. Schematic diagram illustrating mechanism of charge transfer and separation of CeO_2-PANI under visible-light irradiation

To evaluate antibacterial efficacy of CeO_2-PANI, a range of concentrations were systematically investigated, as illustrated in Fig.10. Experimental results revealed that the minimum inhibitory concentration for foodborne bacterial strains was determined to be 100 µg/mL. A concentration dependent increase in antibacterial activity was detected, with momentous inhibition of bacterial proliferation, particularly during exponential growth stage. Conspicuously, at highest concentration tested (400 µg/mL), complete bacterial growth inhibition was accomplished (Fig.10a, b). CeO_2-PANI confirmed persistent antimicrobial potential against foodborne bacteria, emphasizing their broad-spectrum effectiveness. Perceptibly these results indicate that antimicrobial performance is closely linked to both concentration of heterostructure and successful incorporation of CeO_2 NCs within the PANI NT matrix. Mechanistically, antibacterial activity of CeO_2-PANI is accredited to a synergistic interaction of physicochemical progressions. It is anticipated that upon introduction to aqueous environments, the CeO_2 NCs produce reactive oxygen species (ROS), for instance, hydroxyl radicals (•OH), superoxide anions ($O_2•^-$), and hydrogen peroxide (H_2O_2). These ROS induce oxidative stress within bacterial cells, ensuing in lipid peroxidation, protein denaturation, and nucleic acid degradation, eventually triggering cell death. Furthermore, the high aspect ratio structure of CeO_2-PANI heterostructure enables physical distraction of bacterial sheaths, leading membrane penetrability, therefore triggering cytoplasmic seepage. Additionally, the discharge of Ce^{3+}/Ce^{4+} ions interfere with enzymatic activity, bind to vital molecules, impair important metabolic and replication paths, thus collectively contribute to bacteriostatic and bactericidal activity (Ghodake et al., 2025).

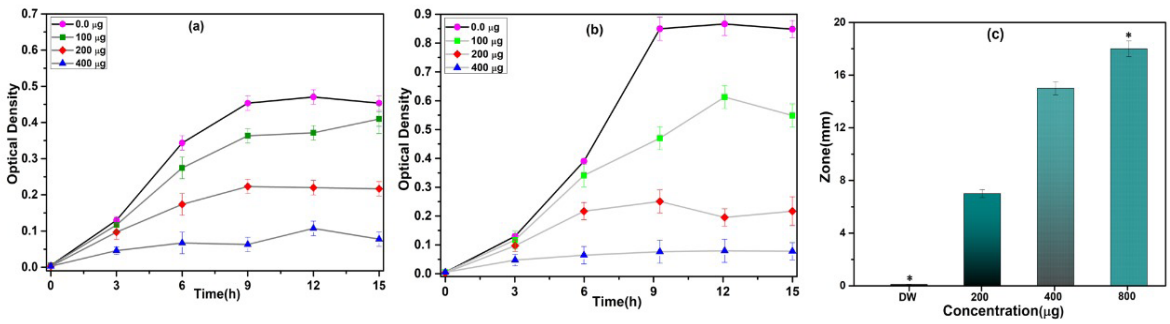


Figure 10. Antimicrobial sensitivity of (a) S. aureus (b) S. typhimurium after 20 h (c) C. albicans fungus after 72 h with CeO_2-PANI heterostructure at different concentrations (0-800 µg/mL). Data imply mean ± SD (*p≤0.05). Statistical calculations were done on Origin Pro2016 software

The matrix of PANI NT provide extra purposeful assistances, such as improved dispersion and equilibrium of CeO_2 NCs, electrochemical reactivity, environmental resilience, and effortlessness of surface amendments. These features style CeO_2-PANI heterostructure a versatile and promising candidate for assimilation into progressive antimicrobial material, such as filtration membranes, protective coatings, or water purification systems. In analog, the anticandidal activity of CeO_2-PANI heterostructure was evaluated by means of broth dilution technique against Candida albicans, designated as an illustrative fungal strain. The MIC was determined to be 100 µg/mL, while a pronounced antifungal effect was detected at higher concentrations, predominantly at 800 µg/mL, as portrayed in Figure 10c. The antifungal mechanism, parallel to antibacterial action, is predominantly driven by ROS production enabled by redox-active Ce^{3+}/Ce^{4+} species under aqueous settings. Likewise, it is expected that these species will dislodge fungal cell membranes, disintegrate crucial proteins, and produce DNA destruction (Fig.11). Amalgamation with PANI NT not only expands bioavailability of CeO_2 NCs but also augments interaction with fungal surfaces due to high aspect ratio and intrinsic electroactivity.

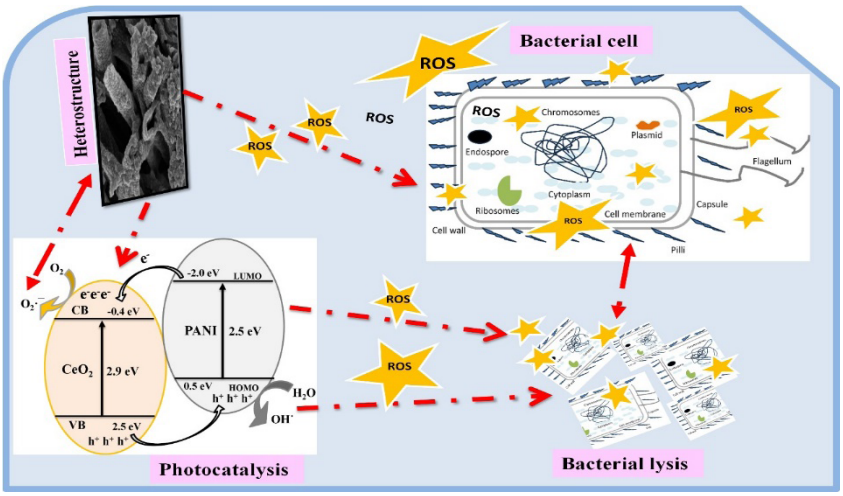


Figure 11. Proposed schematic overview of antimicrobial activity mechanism of CeO_2-PANI heterostructure

Conclusively, the CeO_2-PANI NTs exhibits robust antimicrobial properties via manifold harmonizing mechanisms. Nevertheless, its exclusive physicochemical features, united with exceptional biocidal competence, place them as a next generation nanotextured material for mitigating microbial contamination and ensuring safe, clean water.

4. Conclusion

To sum up, the untreated dye-containing effluents can pollute waterways, damage aquatic ecosystems, and degrade overall water quality. Likewise, pathogenic bacteria will continue to cause outbreaks and fatalities worldwide, as no effective interventions have yet succeeded in eliminating them completely from food supply. Herein the CeO_2-PANI NTs were effectively primed via in situ deposition oxidative polymerization of aniline monomer. The microstructure has been investigated and discussed in detail. The FT-IR results confirmed the interaction between PANI and CeO_2 in heterostructure. This demonstrated compelling absorption in visible light region and exhibited enhanced photocatalytic efficiency for the degradation of Rh6 G dye. A possible photocatalytic and antimicrobial mechanism is proposed. Additional studies are obligatory to progress effective approaches which could be blend of existing practices and those being developed. In this direction, CeO_2-PANI have shown great potential in photocatalysis and antimicrobial applications. This hybrid material synergistically combines redox-active properties of CeO_2 NCs with high surface area and conductive polymer matrix of PANI nanotubes, resulting in enhanced antimicrobial performance. The heterostructure not only inhibits microbial growth but can also prevent biofilm formation on surfaces, a key factor in reducing long-term contamination in water systems. The development of new materials and exploration of their applications in various fields are expected to further enhance their potential and impact in environmental and health sectors.

4.1 Statements and Declarations

1. **Funding**: The authors declare that no funds, grants, or other support were received during the preparation of this manuscript
2. **Data Availability:** The data underlying this article are available in article. The data generated or analyzed during current study are available from corresponding author on request.
3. **Conflict of interest:** The authors declare that they have no conflict of interest. All authors approve the submission.

4. **Ethical approval:** Not applicable.
5. **Compliance with ethical standards:** Not applicable

5. References

1. *Algethami, Jari S, Hassan, M Shamshi, Amna, Touseef, Alqarni, Laila S, Alhamami, Mohsen AM, & Seliem, Amal F. (2023). Bismuth vanadate decked polyaniline polymeric nanocomposites: The robust photocatalytic destruction of microbial and chemical toxicants. Materials, 16(9), 3314.*
2. *Alghamdi, Samia Q, Alotaibi, NF, Al-Ghamdi, Sameera N, Alqarni, Laila S, Amna, Touseef, Moustafa, Shaima MN, . . . Nassar, AM. (2024). High antiparasitic and antimicrobial performance of biosynthesized nio nanoparticles via wasted olive leaf extract. International Journal of Nanomedicine, 1469-1485.*
3. *Amna, Touseef. (2023). Bactericide gold decorated mulberry fibers for therapeutic and non-therapeutic tenacities. Journal of Umm Al-Qura University for Applied Sciences. doi: 10.1007/s43994-023-00032-x*
4. *Amna, Touseef, Hassan, M Shamshi, Nam, Ki-Taek, Bing, Yang You, Barakat, Nasser AM, Khil, Myung-Seob, & Kim, Hak Yong. (2012). Preparation, characterization, and cytotoxicity of CPT/Fe2O3-embedded PLGA ultrafine composite fibers: A synergistic approach to develop promising anticancer material. International journal of nanomedicine, 1659-1670.*
5. *Amna, Touseef, Hassan, M Shamshi, Yousef, Ayman, Mishra, Amrita, Barakat, Nasser AM, Khil, Myung-Seob, & Kim, Hak Yong. (2013). Inactivation of foodborne pathogens by NiO/TiO2 composite nanofibers: A novel biomaterial system. Food and Bioprocess Technology, 6(4), 988-996.*
6. *Chaudhry, Fahad Nazir, & Malik, Muhammad Faisal. (2017). Factors affecting water pollution: a review. J. Ecosyst. Ecography, 7(1), 225-231.*
7. *Cho, Min Seong, Park, Sun Young, Hwang, Ji Yeon, & Choi, Hyoung Jin. (2004). Synthesis and electrical properties of polymer composites with polyaniline nanoparticles. Materials Science and Engineering: C, 24(1-2), 15-18.*
8. *Eng, Shu-Kee, Pusparajah, Priyia, Ab Mutalib, Nurul-Syakima, Ser, Hooi-Leng, Chan, Kok-Gan, & Lee, Learn-Han. (2015). Salmonella: a review on pathogenesis, epidemiology and antibiotic resistance. Frontiers in life science, 8(3), 284-293.*
9. *Ghodake, Vijay S, Koyale, Pramod A, Patil, Satyajeet S, Patil, Pramod S, & Delekar, Sagar D. (2025). Exploring the antibacterial properties of ZnO nanorods-CuO nanoflowers: a mode of action approach. RSC advances, 15(40), 32995-33005.*
10. *Guo, Bingcao, Zhao, Yibo, Wu, Wei, Meng, Hong, Zou, Haikui, Chen, Jianfeng, & Chu, Guangwen. (2013). Research on the preparation technology of polyaniline nanofiber based on high gravity chemical oxidative polymerization. Chemical Engineering and Processing: Process Intensification, 70, 1-8.*
11. *Haleem, Abdul, Ullah, Mohib, Shah, Afzal, Farooq, Muhammad, Saeed, Tooba, Ullah, Ishan, & Li, Hao. (2024). In-depth photocatalytic degradation mechanism of the extensively used dyes malachite green, methylene blue, congo red, and rhodamine B via covalent organic framework-based photocatalysts. Water, 16(11), 1588.*
12. *Hassan, M Shamshi, Khan, Rizwan, Amna, Touseef, Yang, Jiyeong, Lee, In-Hwan, Sun, Min-Young, . . . Khil, Myung-Seob. (2016). The influence of synthesis method on size and toxicity of CeO2 quantum dots: Potential in the environmental remediation. Ceramics International, 42(1), 576-582.*
13. *Hassan, M Shamshi, Tirth, Vineet, Alorabi, Ali Q, Khan, Firoz, Algahtani, Ali, & Amna, Touseef. (2022). Bi2WO6 nanoflakes incorporated carbon nanofibers to control biological and chemical pollutants: bifunctional application. Chemical Engineering Communications, 209(6), 844-851.*
14. *He, Kai, Li, Mingtao, & Guo, Liejin. (2012). Preparation and photocatalytic activity of PANI-CdS composites for hydrogen evolution. International journal of hydrogen energy, 37(1), 755-759.*
15. *Ho, Chunman, Yu, Jimmy C, Kwong, Tszyan, Mak, Angelo C, & Lai, Sukyin. (2005). Morphology-controllable synthesis of mesoporous CeO2 nano-and microstructures. Chemistry of Materials, 17(17), 4514-4522.*
16. *Jalal, Mohammad, Ansari, Mohammad Azam, Ali, Syed Ghazanfar, Khan, Haris M, & Rehman, Suriya. (2018). Anticandidal activity of bioinspired ZnO NPs: effect on growth, cell morphology and key virulence attributes of Candida species. Artificial cells, nanomedicine, and biotechnology, 46(sup1), 912-925.*

17. *Jalal, Mohammad, Ansari, Mohammad Azam, Shukla, Arun Kumar, Ali, Syed G, Khan, Haris M, Pal, Ruchita, . . . Cameotra, Swaranjit Singh. (2016). Green synthesis and antifungal activity of Al 2 O 3 NPs against fluconazole-resistant Candida spp isolated from a tertiary care hospital. RSC advances, 6(109), 107577-107590.*
18. *Jeong, Won-Hui, Amna, Touseef, Ha, Yu-Mi, Hassan, M Shamshi, Kim, Hyun-Chel, & Khil, Myung-Seob. (2014). Novel PANI nanotube@ TiO2 composite as efficient chemical and biological disinfectant. Chemical Engineering Journal, 246, 204-210.*
19. *Kadariya, Jhalka, Smith, Tara C, & Thapaliya, Dipendra. (2014). Staphylococcus aureus and staphylococcal food-borne disease: an ongoing challenge in public health. BioMed research international, 2014(1), 827965.*
20. *Kumbhar, Gajanan Babu, Shingare, Shyamala Prakash, Bagal, Manisha V, Suryawanshi, Mahesh Arjun, & Mane, Vijay Balaso. (2025). Evaluating the Mechanisms of Decolouration and Degradation in Textile Dyes Environmental Impacts and Sustainable Solutions. Environmental Claims Journal, 1-35.*
21. *Li, Xingwei, Chen, Wei, Bian, Chaoqing, He, Jinbo, Xu, Ning, & Xue, Gi. (2003). Surface modification of TiO2 nanoparticles by polyaniline. Applied Surface Science, 217(1-4), 16-22.*
22. *Lotfi, Safia, Ouardi, Mohamed El, Ahsaine, Hassan Ait, & Assani, Abderrazzak. (2022). Recent progress on the synthesis, morphology and photocatalytic dye degradation of BiVO4 photocatalysts: A review. Catalysis Reviews, 1-45.*
23. *Lowy, Franklin D. (1998). Staphylococcus aureus infections. New England journal of medicine, 339(8), 520-532.*
24. *Maliszewska, Irena, & Czapka, Tomasz. (2022). Electrospun polymer nanofibers with antimicrobial activity. Polymers, 14(9), 1661.*
25. *Mohammed, Manal. (2017). Phage typing or CRISPR typing for epidemiological surveillance of Salmonella Typhimurium? BMC research notes, 10(1), 578.*
26. *Phanichphant, Sukon, Nakaruk, Auppatham, & Channei, Duangdao. (2016). Photocatalytic activity of the binary composite CeO2/SiO2 for degradation of dye. Applied Surface Science, 387, 214-220.*
27. *Samai, Boby, & Bhattacharya, Subhash Chandra. (2018). Conducting polymer supported cerium oxide nanoparticle: Enhanced photocatalytic activity for waste water treatment. Materials Chemistry and Physics, 220, 171-181.*
28. *Shamshi Hassan, M, Amna, Touseef, Aljuaid, Alya, Algethami, Jari S, Alqarni, Laila S, & Khil, Myung-Seob. (2024). Cerium oxide nanofibers via electrospinning: a potential material to purge waterways of chemical pollutants and foodborne pathogens. Chemical Papers, 78(12), 6961-6970.*
29. *Sharma, Surbhi, & Khare, Neeraj. (2018). Sensitization of narrow band gap Bi 2 S 3 hierarchical nanostructures with polyaniline for its enhanced visible-light photocatalytic performance. Colloid and Polymer Science, 296, 1479-1489.*
30. *Singu, Bal Sydulu, Srinivasan, Palaniappan, & Pabba, Srinivas. (2011). Benzoyl peroxide oxidation route to nano form polyaniline salt containing dual dopants for pseudocapacitor. Journal of The Electrochemical Society, 159(1), A6.*
31. *Turkten, Nazli, Karatas, Yunus, Kurumoglu, Simal, & Gurkan, Yelda Yalcin. (2025). Enhanced Photocatalytic Degradation of Diazo Reactive Blue 198 Using Ternary PANI-TiO2-CuO Composites: Predicted Degradation Pathway, Mechanism, and DFT Calculations. Physica B: Condensed Matter, 417802.*
32. *Wang, Hongjuan, Yang, Lin, Yu, Hao, & Peng, Feng. (2011). A Highly Efficient and Stable Visible-Light Plasmonic Photocatalyst Ag-AgCl/ CeO 2. World Journal of Nano Science and Engineering, 1(04), 129.*
33. *Wang, Qizhao, Hui, Juan, Li, Jiajia, Cai, Yuxia, Yin, Shuqun, Wang, Fangping, & Su, Bitao. (2013). Photodegradation of methyl orange with PANI-modified BiOCl photocatalyst under visible light irradiation. Applied Surface Science, 283, 577-583.*
34. *Yu, Wen Jie, Cheng, Yang, Zou, Tao, Liu, Yi, Wu, Kui, & Peng, Na. (2018). Preparation of BiPO4-polyaniline hybrid and its enhanced photocatalytic performance. Nano, 13(01), 1850009.*